Antiferromagnetic Single-Chain Magnet slow relaxation in the polymer $\{Ln(\alpha\text{-fur})_3\}_n$ with Ln=Tb(III) non-Kramers ion

E.Bartolomé[a] , J. Bartolomé[b] , A. Arauzo[b,c], J. Luzón[d], L. Badía[b], R. Cases[b], F. Luis[b] , S. Melnic[e], D. Prodius[e], S. Shova[f] and C. Turta[e+]

We report the synthesis, crystal structure and magnetic properties of a new molecular complex based on a Tb ion, supported by 2-furancarboxylic molecules: $\{Tb(\alpha\text{-fur})_3(H_2O)_3\}_n$ (α-fur= C_4H_3OCOO). Two slightly different Tb sites (A and B), exist depending on the position of one of the dangling ligands. *Ab initio* calculations predict that, for both sites, the magnetic ground state is highly anisotropic (g_z*=17.8) and consists of a quasi-doublet with a small gap, well separated from the next excited state. The α-fur ligand forms 1D polimeric chains of Tb ions of the same type (either A or B) running along the *c*-axis. The crystal structure is formed by the supramolecular stacking along the *a*-axis of 2D layers containing parallel chains of the same type. Static magnetization and heat capacity measurements show that, magnetically, the system can be modeled as an ensemble of Ising chains of non-Kramers Tb ions with effective spin S*=1/2, antiferromagnetically (AF) coupled by a weak intrachain interaction (J^*/k_B =-0.135 K). At very low temperatures, the static susceptibility reflects the presence of a 2-4% concentration of defects in the chains. Ac susceptibility measurements in *H*=0 performed down to mK temperatures have enabled us to observe slow relaxation of the magnetization through two different pathways. They are assigned to Single-Chain-Magnet (SCM) behavior in the two different types of AF chains (A and B), triggered by the existence of defects breaking the chains in segments with short-range order. At temperatures below 0.1 K this mechanism is replaced by individual relaxation of the ions through direct processes. Under the application of a magnetic field the system slowly relaxes by two distinct direct processes, strongly afected by a phonon bottleneck effect.

Introduction

The field of molecule-based multifunctional materials has quickly advanced in recent years. Low-dimensional magnetic systems, such as single-ion magnets (SIMs)[1], single-molecule magnets (SMMs)[2] and single-chain magnets (SCMs)[3–5] are being thoroughly investigated, due to their fundamental interest and potential application in information storage, quantum computing, switching, magneto-optics etc[6].

The slow-relaxation dynamics of such complexes is caused by the existence of an energy barrier between two stable states. While the barrier height for the reversal of the magnetization in SIMs and SMMs depends mainly on their spin ground-state and magnetic anisotropy, in SCMs it is additionally affected by intrachain interactions between the constituent magnetic entities and by the presence of defects. Sufficiently large interchain interactions at low temperatures can even produce 3D long-range ordering, not necessarily suppressing the SCM dynamics[7,8]. Moreover, for certain complexes, slow relaxation towards equilibrium is replaced at adequate fields and temperatures by fast relaxation through quantum tunnelling.

One-dimensional (1D) lanthanide-based complexes represent an ideal playground to study how slow dynamics and tunnelling depend on the type of ion and its coordination sphere, the relative importance of the ion's anisotropy vs. exchange, and the nature, sign and intensity of intrachain / interchain competing interactions. Thus, our recent research has been focused on the investigation of relaxation processes in lanthanide (III) polymeric furoates by means

[a.] *Escola Universitària Salesiana de Sarrià (EUSS), Passeig Sant Joan Bosco 74, 08017-Barcelona, Spain. Fax: +34 932806642; Tel: +34-932805244; E-mail: ebartolome@euss.es*
[b.] *Instituto de Ciencia de Materiales de Aragón, CSIC-Universidad de Zaragoza, Pedro Cerbuna 12, 50009 Zaragoza, Spain.*
[c.] *Servicio de Medidas Físicas. Universidad de Zaragoza, Pedro Cerbuna 12, 50009 Zaragoza, Spain.*
[d.] *Centro Universitario de la Defensa. Academia General Militar, Zaragoza, Spain*
[e.] *Institute of Chemistry, Academy of Sciences of Moldova, Academiei 3, MD-2028, Chisinau, Republic of Moldova*
[f.] *Institute of Macromolecular Chemistry "Petru Poni" Iasi, Aleea Grigore Ghica Voda, nr. 41A, 700487 Iasi, Romania*

of very low temperature ac susceptibility experiments. On one hand, owing to their especial electronic properties, trivalent lanthanides are especially well suited for building slow relaxing systems. On the other hand, the α-fur=C_4H_3OCOO ligand, acting in bridging mode, is efficient in consolidating stable 1D chains containing rare earths[9]. We have recently reported the synthesis and characterization of {Ln(α-fur)$_3$}$_n$, with Ln=Dy[10] and Nd[11], and heteronuclear {[Dy_2Sr(α-fur)$_8$(H_2O)$_4$]}$_n$·2H_2O[12] and {Dy_2Ba(α-fur)$_8$}$_n$[13]. So far, all the studied complexes were based on Kramers ions (Ln=Dy, Nd), i.e. with odd number of electrons at the 4f orbitals. In this work we expand our efforts to complexes based on a non-Kramers ion (i.e. with an even number of electrons at the 4f orbitals) like Tb, since time parity has a bearing on the relaxation processes, for example on tunnelling.

Tb(III) has been one of the preferred lanthanides for the synthesis of SIMs[1,14–16], SMMs[17–20] or SCMs[8,21,22] because its large intrinsic magnetic anisotropy favors slow relaxation of the magnetization[23]. Interestingly, Tb(III) complexes may be also used as luminescent agents, provided the Tb cation can be efficiently sensitized by an attached Ln'-ligand "antenna"[24]. Most of the reported slow relaxing Tb chains present 1D Ising character and dominant intrachain ferromagnetic interactions[25]; in some cases 3D long-range ordering is reached thanks to antiferromagnetic (AF) interchain coupling[8,26]. Recently, some hints of slow relaxation were found at very low temperatures in a [Tb(hfac)$_3$(NIT2-PyOCH$_3$)] complex with AF intrachain coupling[27].

In this paper we report the synthesis and magneto-structural characterization of a new 1D α-furoate compound, {Tb(α-fur)$_3$}$_n$. Ac measurements performed down to mK temperatures have allowed us to unveil slow relaxation of the magnetization in the absence of magnetic field in this complex. This is to our knowledge, the first example of a transverse Ising AF chain constituted by non-Kramers ions displaying slow relaxation dynamics.

Synthesis and structural characterization

The complex was synthesized by using the furoic acid as polydentate O-donor carboxylic acid in aqueous media. Reaction between a mixed Tb(III)/Sr(II) complex and the lanthanide sulfate leads to the formation of the homonuclear complex {Tb(α-fur)$_3$(H_2O)$_3$}$_n$. The starting {[Tb_2Sr(α-fur)$_8$(H_2O)$_4$]}$_n$·2H_2O complex was obtained according to the synthetic protocol reported in our previous work[12].

Crystallographic measurements for {Tb(α-fur)$_3$(H_2O)$_3$}$_n$ were performed on an Oxford-Diffraction XCALIBUR E CCD diffractometer using Mo Kα radiation selected by a graphite monochromator. The single crystal was positioned at 40 mm from the detector and 222 frames were measured each for 8 and 10 s over 1° scan width. The unit cell determination and data integration were carried out using the Oxford Diffraction CrysAlis package[28]. The structure was solved by direct methods using Olex2[29] software with the SHELXS structure solution program and refined by full-matrix least-squares on F² with SHELXL-97[30].

Table 1. Crystallographic data, details of data collection and structure refinement parameters for {Tb(α-fur)$_3$}.

	{Tb(α-fur)$_3$} CCDC-1438518
Empirical formula	$C_{15}H_{15}O_{12}Tb$
Formula weight	546.19
Temperature/K	293
Crystal system	monoclinic
Space group	*C*2/*c*
a/Å	22.1451(8)
b/Å	16.0302(6)
c/Å	10.2110(4)
α/°	90.00
β/°	100.040(4)
γ/°	90.00
V/Å^3	3569.3(2)
Z	8
D_{calc}/mg/mm^3	2.033
μ/mm^{-1}	4.028
Crystal size/mm^3	0.50 × 0.20 × 0.20
ϑ_{min}, ϑ_{max}(°)	3.16 to 50.04
Reflections collected	6723
Independent reflections	3144 [R_{int} = 0.0439]
Data/restraints/parameters	3144/108/235
GOF[c]	1.073
R_1[a]($I>2\sigma(I)$)	0.0396
wR_2[b](all data)	0.0989
Largest diff. peak/hole/e Å^{-3}	0.85/-0.84

[a] $R_1 = \Sigma||F_o| - |F_c||/\Sigma|F_o|$, [b] $wR_2 = \{\Sigma[w(F_o^2 - F_c^2)^2]/\Sigma[w(F_o^2)^2]\}^{1/2}$.

[c] GOF = $\{\Sigma[w(F_o^2 - F_c^2)^2]/(n-p)\}^{1/2}$, , where *n* is the number of reflections and *p* is the total number of parameters refined

Table 2. Selected bond distances for {Tb(α-fur)$_3$}.

	Distance (Å)
Tb1-O1	2.307(4)
Tb1-O1*w*	2.399(5)
Tb1-O2^1	2.329(4)
Tb1-O2*w*	2.542(4)
Tb1-O3*w*	2.464(13)
Tb1-O4*w*	2.506(16)
Tb1-O4	2.295(4)
Tb1-O5^2	2.358(5)
Tb1-O7x	2.372(14)
Tb1-O7	2.395(13)
O1-C1	1.244(6)
O2-C1	1.244(6)
O3-C2	1.375(6)
O3-C5	1.370(6)
O4-C6	1.242(6)
O5-C6	1.247(6)
O6-C7	1.380(6)
O6-C10	1.365(6)
O8-C11	1.284(15)

Symmetry codes: (1) -3/2-*X*, -3/2- *Y*, -2-*Z*; (2) -3/2 -*X*, -3/2 -*Y*, -1 -*Z*

Atomic displacements for non-hydrogen atoms were refined using an anisotropic model. All H atoms attached to carbon were introduced in idealized positions (d_{CH} = 0.96 Å) using the riding model with their isotropic displacement parameters fixed at 120% of their riding atom. Positional parameters of the H attached to O atoms were obtained from difference Fourier syntheses and verified by the geometric parameters of the corresponding hydrogen bonds. One of the furoic acid ligands and one of the coordinated water molecules were found to be statistically disordered over two resolvable interchanged positions with equal occupancy. The positional parameters of these atoms were refined using available tools (PART, DFIX, and SADI) of SHELXL-97 and the combined anisotropic/isotropic refinement has been applied for non-hydrogen atoms. The molecular plots were obtained using the Olex2 program. Table 1 provides a summary of the crystallographic data together with refinement details for the new compound. CCDC-1438518 contains the supplementary crystallographic data for this contribution, which can be obtained, free of charge via www.ccdc.cam.ac.uk/conts/retrieving.html (or from the Cambridge Crystallographic Data Centre, 12 Union Road, Cambridge CB2 1EZ, UK; fax: (+44) 1223-336-033; or deposit@ccdc.ca.ac.uk). The single crystal X-ray study has demonstrated that the compound reported in this paper along with that of Dy one, which we reported earlier[10], form a series of isomorphous coordination polymers with the general formula $\{Ln(C_4H_3OCOO)_3(H_2O)_3\}n$.

The results of the X-ray crystallography analysis are presented in Figure 1 while selected interatomic distances are quoted in Table 2. The coordination position of the disordered carboxylate, which behaves as a deprotonated monodentate ligand, is shared by a water molecule equally distributed within the same coordination sites. Therefore, depending on the position of disordered ligands, Tb atom exhibits two different but very similar coordination environments, hereafter referred to as Tb(A) and Tb(B) (Fig. 1). Each terbium ion is coordinated by oxygen atoms originating from carboxylate groups and water molecules, showing a coordination number of eight. Fig. 1 illustrates the coordination polyhedron of the Tb atom, which can be described as a distorted bicapped trigonal prism for both disordered positions of the ligands. Three carboxylate ligands adopt two different coordination modes in the crystal. Two of them are coordinated in bidentate-bridging mode (Fig. 2) and the other one acts as a monodentate ligand being coordinated through oxygen atom O7 (O7x). At the same time, the second oxygen atom of the monodentate carboxylate groups O8 (O8x) are involved in the formation of H-bonds with the O2*w* (O1*w*, respectively) coordinated water molecules. Within the coordination polyhedron the Ln-$O_{bridging}$, Ln-$O_{monodent}$ and Ln-O_{water} interatomic distances are in good agreement with whose found for Dy complex[10].

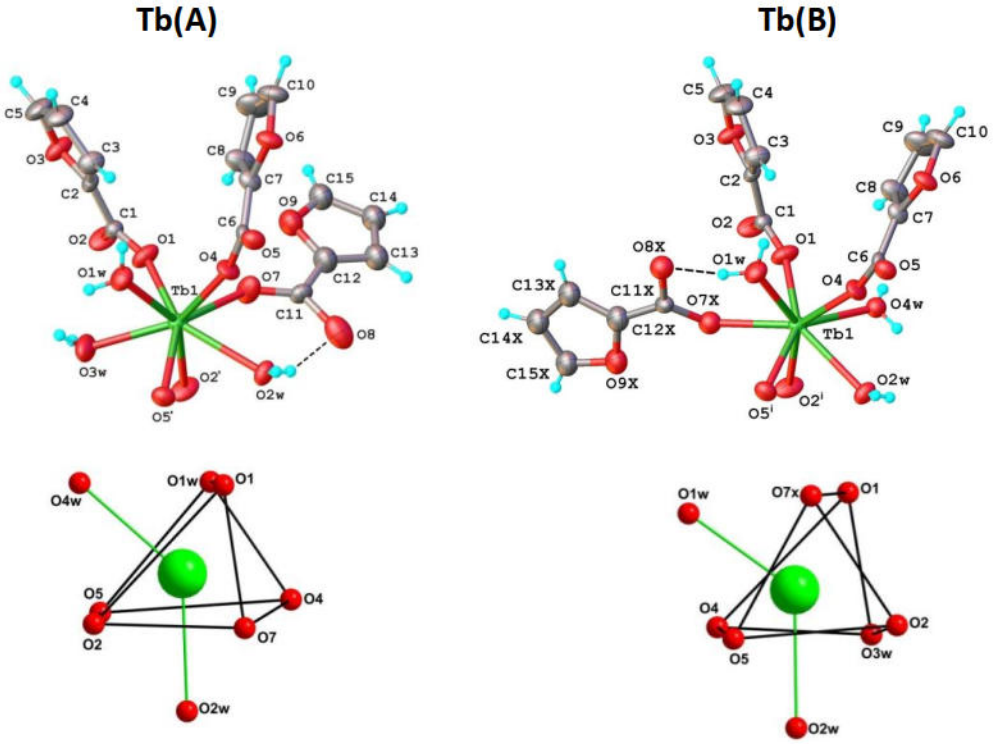

Figure 1. Two coordination environments of the Tb atom according to two positions of disordered ligands, Tb(A) and Tb(B). Thermal ellipsoids are drawn at 50% probability level. Suffix "x" denotes disordered position of the furoate ligand. Symmetry code for the equivalent atoms: (1)-1.5 – *X*, -0.5 – *Y*, 2 – *Z*.

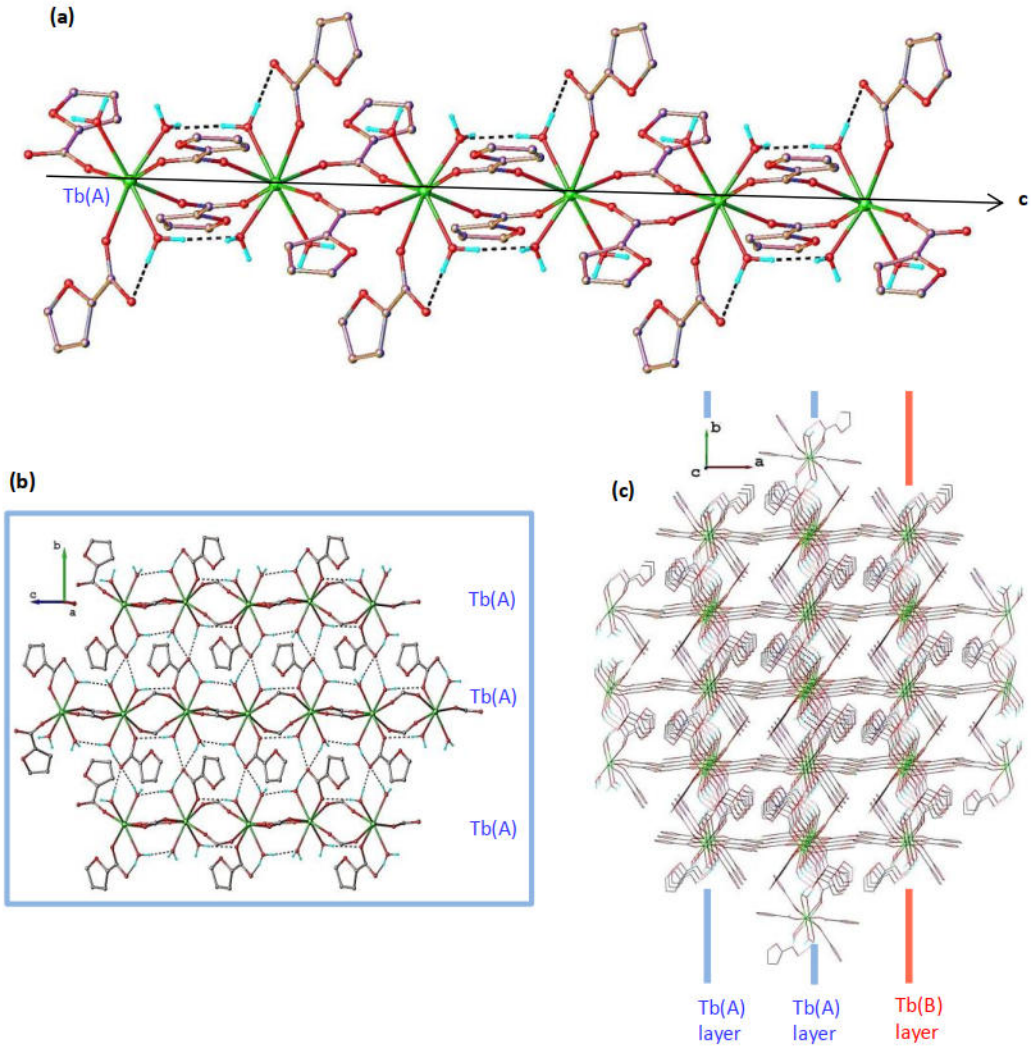

Figure 2. (a) Perspective view of a 1D coordination polymer formed by only one type of the disordered components, Tb(A); similarly, 1D chains containing only Tb(B) ions are formed. Non-relevant H-atoms are omitted for clarity; (b) 2D supramolecular layers are formed by the coordination of similar type of chains (e.g. Tb(A) chains in the figure). Some atoms of furoate cycles are omitted for clarity; (c) view of crystal along *a*-axis showing packing of Tb(A) and Tb(B) 2D supramolecular layers.

In the crystal, the asymmetric part is linked via the inversion center into the neutral polymeric chains running along *c* direction, as shown in Fig. 2a. The formation of this polymeric architecture is additionally strengthened by the intramolecular H-bonds that occur between water molecules coordinated to adjacent Tb atoms. The separations between two Tb ions within the coordination polymer are of 5.196(1) Å and 5.035(1) Å. In turn, the coordination polymers are further interacting in the crystal via H-bonding formed between coordinated water molecules and non-coordinated oxygen atoms of the mono-coordinated carboxylate groups. It results into the formation of two distinct 2D supramolecular layers differing by the orientation of disordered carboxylate ligands. One of these 2D supramolecular layers in the *bc*-plane, containing Tb(A)-only chains, is depicted in Fig. 2b. The crystal structure is generated by the random, alternating packing of Tb(A) and Tb(B) types of supramolecular layers, as shown in Fig. 2c. Each of these layers contains chains of identical Tb (type A or B) running along the *c*-axis (See Fig. 2c)

Ab initio simulations

In order to determine the energy level structure of the Tb(III) multiplet ground state and the main axes of the effective gyromagnetic *g**-tensor for the two lowest states, relativistic *ab initio* calculations were performed using the CASPT2/RASSI-SO[31] method as implemented in the MOLCAS 7.8 package[32]. Due to the positional disorder between a water molecule and a furoic ligand, there are two slightly different environments for the Tb(III) ion. Therefore, *ab initio* calculations were performed on two molecular clusters in which the atomic positions were extracted from the X-ray crystal structure. The cluster models include the central Tb ion and two La(III) ions in the positions of the two neighbour Tb(III) ions along the *c* crystallographic axis. The models also include the furoic ligands and water molecules surrounding the studied Tb(III) ion and the water molecules surrounding the two neighbour Tb(III) ions. In order to reduce the computation time, without a significant loss of accuracy, the furoic acid ligands around the two neighbour Tb(III) ions have been replaced by -0.5 point charges. The replacement of the neighbour Tb(III) ion by an La(III) ion is done in order to reduce the active space. After

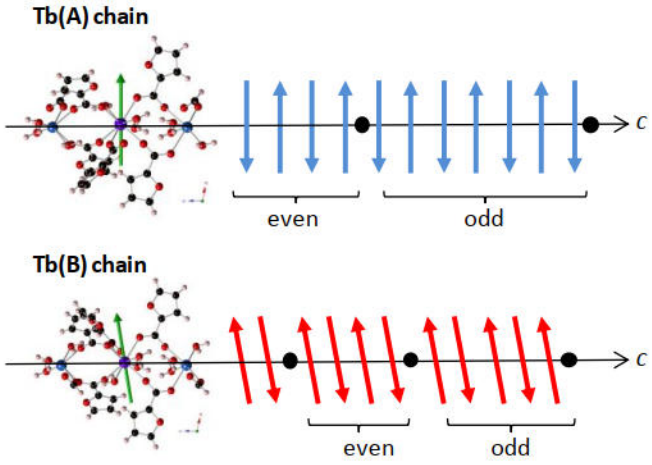

Fig. 3. *Ab initio* calculated easy anisotropy axes for Tb(A) and Tb(B) sites, almost perpendicular to the *c*-axis; Schematics of the distinct Tb(A) and Tb(B) chains with AF coupled ions. Defects break chains in segments with either even or odd number of spins.

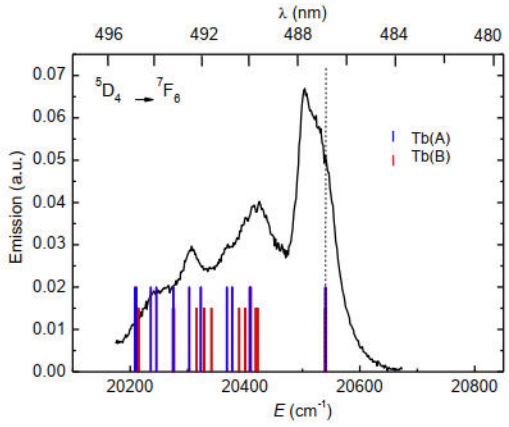

Fig. 4. Emission spectrum of {Tb(α-fur)$_3$} at 77 K compared to the electronic energy level scheme predicted by *ab initio* calculations.

that, the chosen CASSCF active space consisted of the Tb 4f orbitals, containing 8 electrons in seven orbitals [CASSCF(8,7)]. An averaged-state CASSCF calculation was done on the 7F septets (7 roots) and then a CASPT2 correction was applied.

We have calculated by *ab initio* methods the eigenfunctions of the four lowest ligand field split energy levels for the two different terbium sites, Tb(A) and Tb(B). Results are presented in Table S1 and S2. The ground state, $|\xi_0\rangle = \sum_{M=-J}^{J} C^0_{J,M_J}|J,M_J\rangle$, is dominantly composed of state $|J,M_J\rangle = |6,\pm6\rangle$ with some mixture from $|6,\pm5\rangle$. The calculations predict that the energies of the first excited state, $|\xi_1\rangle = \sum_{M=-J}^{J} C^1_{J,M_J}|J,M_J\rangle$ and of the ground state differ by a small energy gap, very similar for the two Tb sites, (Δ_A/k_B =0.201 K and Δ_B/k_B =0.258 K). Therefore the ground state can be considered as a quasi-doublet. The energy of the second excited state, $|\xi_2\rangle$, is also very similar for the two sites, E_{2A}/k_B =185.9 K and E_{2B}/k_B =168.8 K respectively.

For the quasi-doublet ground-state, *ab initio* calculations of the effective gyromagnetic ratios along the main single-ion anisotropy axes indicate a large uniaxial magnetic anisotropy, with g_z*=17.8, g_x*=g_y*≈0 for the two sites, within an effective S*=1/2 ground state description, which is applicable at sufficiently low temperatures. This result is expected for a non-Kramers ion with two non-degenerate states at low energy and the next excited levels at much higher energy[33]. Besides, simulations indicate that the EAM is nearly perpendicular to the *c*-axis (Fig. 3): 87.9° and 80.1° for Tb(A) and Tb(B), respectively. The calculated dipolar interaction along a chain is AF, with a magnitude of J_{dip}/k_B≈-0.8K.

Photo-physical properties

After exciting the complex from its $^7F_6$ to its $^5D_3$ levels with 380 nm wavelength photons, it undergoes de-excitation from the $^5D_3$ to the $^5D_4$ multiplet and subsequent radiative decay from the $^5D_4$ to the ^7F_J low lying states. Fig. 4 shows the $^5D_4 \rightarrow {}^7F_6$ emission spectrum measured at 77 K. Several components of the multiplet are clearly seen and are compatible with the low symmetry of the Tb environment. For comparison, the figure shows also the sublevels of the $^7F_6$ fundamental multiplet calculated by *ab initio* methods. The multiplet has 13 components although the first two sublevels can be considered as a quasi-doublet (Table S4). The distribution of the calculated sublevels coincides fairly well with the width and components of the $^5D_4 \rightarrow {}^7F_6$ emission band. The energy difference between the most intense peak and the second peak amounts to 122 cm^{-1} (174 K), which is pretty close to the *ab initio* predicted energy difference between the quasi-doublet and the next excited level, $(E_2-E_{0,1})/k_B$ = 185.9 and 168.8 K, for Tb(A) and Tb(B). Therefore, the low temperature emission spectrum of {Tb(α-fur)$_3$} supports the *ab initio* predictions.

Theoretical model

In this section we present the model that will be applied to analyze the thermo-magnetic results; the theoretical treatment of chains coordinating Tb(III), a non-Kramers ion, deserves some special attention.

Static properties of a non-Kramers Tb(III) chain

The magnetism of Tb(III)-complexes[34] is determined by the strong anisotropy and partially filled 4*f* orbital of the ion. Tb(III) free ion has a structure [Xe]4f^8 (S=3, L=3). The ground state J=6 contains 2J+1=13 degenerate $|J,M_J\rangle$ electronic substates, and due to the large L-S coupling, it is separated by a large energy (thousands of K) from the next excited level with J=5.

The ligand field (LF) lifts the degeneracy of the 2J+1 substate of the ground state multiplet. To determine the LF split eigenstates and eigenvalues from *ab initio* calculations, as we have done (*vide supra*), the LF eigenstates are expressed as linear combinations of the $|J,M_J\rangle$ (J=6,M_J=+6, ..., -6) angular

moment wave functions with respect to the quantization axis, defined by the principal axis of the *g** tensor: $|\xi_i\rangle = \sum_{M=-J}^{J} C^i_{J,M_J} |J, M_J\rangle$.

Typically, the ground state singlet $|\xi_0\rangle$ and the first excited one $|\xi_1\rangle$ are separated by an energy $E_1 \equiv \Delta$ (a few K or less) much smaller than the energy E_2 of the next state $|\xi_2\rangle$ (hundreds of K). Thus, at sufficiently low temperatures $k_B T << E_2$ we only need to consider the two lowest states (quasi-doublet). The single ion LF Hamiltonian can be expressed in this subspace as:

$$\hat{H}_{LF}^{*} = \Delta \begin{pmatrix} 00 \\ 01 \end{pmatrix}, \qquad [1]$$

where the asterisk indicates the projection on the two lowest states. In the case of ions with an even number of unpaired electrons, such as Tb(III), it has been shown[33] that when the excited states above the quasi-doublet are at much higher energy, thus avoiding the mixing of states, the ground state has uniaxial anisotropy. This result is actually obtained in our *ab initio* calculations with $g_z^* \neq 0$, $g_x^* = g_y^* = 0$, with *z* nearly perpendicular to the *c* crystallographic direction (see Table S5)

For *H*=0, the restricted basis $|\xi_0\rangle$ and $|\xi_1\rangle$ diagonalizes the LF Hamiltonian, but a basis transformation that diagonalizes the Zeeman splitting under an intense applied magnetic field is convenient:

$$|\eta\rangle = \frac{1}{\sqrt{2}}(|\xi_0\rangle + |\xi_1\rangle) \text{ and } |\Sigma\rangle = \frac{1}{\sqrt{2}}(|\xi_0\rangle - |\xi_1\rangle), \qquad [2]$$

that maximizes the $\hat{J}_z$ eigenvalues:

$$\hat{J}_Z|\eta\rangle \approx +6|\eta\rangle \text{ and } \hat{J}_Z|\Sigma\rangle \approx -6|\Sigma\rangle. \qquad [3]$$

These two functions span a restricted subspace of the complete basis set that can be projected onto a fictitious basis states S*=1/2:

$$|\eta\rangle \rightarrow |1/2, +1/2\rangle \text{ and } |\Sigma\rangle \rightarrow |1/2, -1/2\rangle. \qquad [4]$$

The effective spin Hamiltonian, including the ligand field and Zeeman splitting becomes:

$$\hat{H}^{*} = \hat{H}_{LF}^{*} + \hat{H}_{z}^{*} = \Delta \hat{S}_{\perp}^{*} + g_z^* \mu_B H \hat{S}_z^*, \qquad [5]$$

acting on the effective base $|S^*, \pm S_z^*\rangle = |1/2, \pm 1/2\rangle$; here $g_z^* = 2 g_J J$. The EAM is nearly perpendicular to the crystallographic *c*-axis (see Fig. 3). Besides, there are two Tb sites with slightly different energy gaps, Δ_A and Δ_B, but in each chain all Tb are of the same type. Thus the LF Hamiltonian for each chain would be:

$$\hat{H}_{LF(A,B)}^{*} = \sum_{i=1}^{N} \Delta_{A,B} \hat{S}_{i,\perp}^{*}, \qquad [6]$$

where i runs along the chain sites.

XRD combined with *ab initio* calculations indicate that there are two types of chains, A and B, in which the magnetic moments are parallel (or antiparallel) to the EAM of the Tb ion, and nearly perpendicular to the chain *c*-direction (Fig. 3). Since along the chain there are two different Tb-Tb distances (Fig. 2a), in principle we consider two different intrachain interaction constants. The magnetic model system can be described as made of dimers with intradimer exchange *J'*, interacting with adjacent dimers along the chain with *J''*. An Ising interaction can be used because of the strongly anisotropic character of the Tb moments, whose moments are nearly aligned along the *a* crystallographic axis. Therefore, the magnetic chain formed by dimers with Ising S*=1/2 spins fulfills the Alternating Bond Chain (ABC) model.

However, when *J**=*J'*=*J''* the ABC model becomes the Ising chain with identical intrachain exchange constants. This case is applicable to the present {Tb(α-fur)$_3$} compound since the intracahin Tb-Tb distances are nearly identical. Thus, we apply the Ising Hamiltonian for S*=1/2 Ising interaction:

$$\hat{H}_{ABC}^{*} = -2 \sum_{i=1}^{N} J^{*}(i, i+1) S_{i,z}^{*} S_{i+1,z}^{*}, \qquad [7]$$

and:

$$\hat{H}_{z}^{*} = \sum_{i=1}^{N} \mu_B g_{i,z}^{*} S_{i,z}^{*} H \cos\theta, \qquad [8]$$

is the Zeeman term for a constant magnetic field applied at an angle θ with respect to the atomic anisotropy axis.

Thus, the chain Hamiltonian under a field is finally given by:

$$\hat{H}_{chain}^{*} = \hat{H}_{LF}^{*} + \hat{H}_{ABC}^{*} + \hat{H}_{z}^{*} = \hat{H}_{TIC}^{*} + \hat{H}_{z}^{*}, \qquad [9]$$

where $\hat{H}_{TIC}^{*}$ corresponds to the so called transverse Ising chain model (TIC) with S*=1/2.

The static magnetic susceptibility of the TIC model has not been solved yet, to our knowledge. However, it has been shown that the longitudinal susceptibility of an S*=1/2 Ising chain in the presence of a LF anisotropy does not depend on the anisotropy constant[35]. Therefore, we obtain an excellent fit of the susceptibility at *H*=0, *f*=0.3 Hz (nearly static susceptibility limit), with the ABC model expression:

$$\chi_{ABC}^{z} = \frac{N_A g_z^{*2} \mu_B^2}{2 k_B T \left[2 \exp\left(-J^{*}/k_B T \right) \right]}, \qquad [10]$$

for one Tb ion per formula unit. The possible effect of the interchain interactions, $|z_3 J_3|$, is considered under the mean-field approximation:

$$\chi^z_{3D} = \frac{\chi^z_{ABC}}{1 - \frac{z_3 J_3 S_z^2}{N_A g_z^{*2} \mu_B^2} \chi^z_{ABC}}, \quad [11]$$

and for measurements performed on a powder:

$$\chi_{powder} = \chi^z_{3D} / 3 . \quad [12]$$

Note that, since the coupling is AF in this case (*vide infra*), no correction for demagnetization factors is needed.

At very low temperatures, T<0.1 K, an upturn in the susceptibility is observed associated to the inevitable presence of defects in the chain, breaking it in segments of finite length. Segments containing an odd number of spins contribute as one spin to the parallel susceptibility; for a concentration of defects c, such that the number of segments with odd number of spins is $c/2$, the added parallel susceptibility is then[3,4]:

$$\chi_{//} = \frac{c}{2}\frac{C}{T}, \quad [13]$$

where C is the Curie constant.

We have also calculated the equilibrium heat capacity (HC) for our non-Kramers chain. The expression for the HC under the ABC model was explicitly given in Ref.[13] (note *amenda* in Eq. 6 therein). When the LF is additionally considered in the Hamiltonian, as in Eq. [9], the HC (under H=0) can be deduced from the expressions for the free energy previously given for a transverse Ising chain[36], yielding the expression:

$$C/R = \int_0^{\pi} \frac{dq}{\pi} \left(\frac{\varepsilon}{k_B T}\right)^2 \mathrm{sech}^2\left(\frac{\varepsilon}{k_B T}\right), \quad [14]$$

per one Tb atom per formula unit, where $\varepsilon = \sqrt{(J^*/2)^2 + J^* \Delta / 2 \cos q + (\Delta/2)^2}$.

At very low temperatures and under a strong magnetic field we notice that the HC exhibits an increase for decreasing temperature (*vide infra*) that can be only explained as caused by the hyperfine contribution. Then it is considered that Tb(III) has a nuclear spin of I=3/2, in natural abundance of 100%, yielding (2I+1)=4 substates $M_I = -3/2, -1/2, 1/2, 3/2$ The strong hyperfine interaction between the nuclear spin I and J=6 adds a contribution to the Hamiltonian:

$$\hat{H}_{hyp} = A_{dip} I \cdot J + P_{quad}\left(I_z^2 + \frac{1}{3} I(I+1)\right), \quad [15]$$

where the first two terms are caused, respectively, by the nuclear dipole and quadrupole interactions; at $H \neq 0$, an additional nuclear Zeeman term appears:

$$\hat{H}_{Z,I} = -\sum_i^N g_N \mu_N H \hat{I} \quad [16]$$

In summary, the states of the Tb(III) ion within the complex can be described by the total wave functions $\Psi_{ij} \propto |J, M_J\rangle |I, M_I\rangle$, combining the electronic and nuclear wave functions. At high fields, such that the electronic splitting Δ can be expected to be small (≈1 K) with respect to the Zeeman splitting, and considering negligible the quadrupole term, the hyperfine terms Eq. 15 and 16 have to be added to Eq. 9:

$$\hat{H}^* = \hat{H}^*_{ABC} + \hat{H}^*_z + \hat{H}_{hyp} + \hat{H}_{z,I} \quad [17]$$

where g_z*≈18, g_N=1.342, acting on the combined, effective wave functions $\Psi^*_{ij} = |S^*, S^*_z\rangle |I, M_I\rangle$; $S^*_z = 1/2$.

Dynamic properties of AF non-Kramers Tb(III) chain

The relaxation behavior of the one-dimensional system as collective SCM or as an ensemble of decoupled SIMs will depend on the relative intensity of intrachain coupling *vs*. local anisotropy. In addition, the presence of defects is determinant in enabling SCM behavior in AF chains, but at the same time limits the possibility of the system to reach 1D long-range ordering at T=0[4]. We discuss in the following subsections the theoretical treatment of, first, the dynamic relaxation of individual non-Kramers ions, and second, defect-mediated SCM slow relaxation in AF chains of non-Kramers ions.

Relaxation of non-Kramers ions

Slow relaxation of the individual Tb ions can in principle occur via a direct, Raman or Orbach processes. The direct process involves the de-excitation of the electronic state $|\xi_1\rangle$ to the $|\xi_0\rangle$ ground singlet emitting a single phonon that is absorbed by a lattice vibrational mode. Its temperature dependence is given by the expression for a non-Kramers ion with ZFS energy Δ[37]:

$$\tau_d = \tau_0 \tanh(\Delta / k_B T), \quad [18]$$

For the Raman process, the temperature dependence of the relaxation time is approximately given by a power law:

$$\tau_R = B T^{-7}, \quad [19]$$

while for a two phonon Orbach process involving thermal excitation to a third intermediate electronic state with energy E_a it becomes exponential:

$$\tau_{Or} = C\,exp\left(E_a / k_B T\right). \qquad [20]$$

For a non-Kramers ion, slow relaxation through direct processes within the ground state quasi-doublet has a high probability, whereas Orbach processes will be precluded if the first excited state is well separated from the quasi-doublet, as it is in fact our case.

Tunnelling. Relaxation of the individual ions can alternatively occur through fast, tunnelling processes. In the case of Kramers ions, pure quantum tunnelling between the degenerate doublet ground state is forbidden, unless an external perturbation, ξ_{dip}, caused by dipolar, hyperfine or external field allow it. For non-Kramers ions, by contrast, the ZFS energy gap between the quasi-doublet plays the role of a bias field, that may fall within the threshold of $\xi_{bias} = \Delta + \xi_{dip} \leq \Delta_t$ for tunnelling to take place. Here ξ_{dip} encompasses perturbations due to dipolar, exchange and hyperfine interactions, while Δ_t contains the effects of transversal magnetic fields. Under these conditions the prediction for the tunnelling rate through the lowest two states is:

$$\tau_t \approx \frac{\hbar}{\Delta_t^2 P\left(\xi_{dip}\right)}. \qquad [21]$$

The Tb nuclear moment I=3/2 coupled to the electronic states yields an important effect to the bias field and may enhance the tunnelling probability.

Thermally activated quantum tunnelling (TAQT) has the same temperature dependence as an Orbach process (Eq. 20), provided there exist excited degenerate electronic levels. In our complex, none of these processes were observed.

Defect-mediated SCM behaviour in AF chains

Prototypical ferromagnetic Ising chains show slow spin-lattice relaxation when narrow domain walls move along the chain, according to Glauber's model[38]. Though much less common, collective slow relaxation can also occur in AF chains, allowed either by AF canting of spins[3] or by the inevitable existence of defects, breaking the chain in segments with odd and even number of ions.

In a 1D system, critical slowing of the magnetization occurs as the temperature approaches long range ordering (correlation length $\varepsilon \to \infty$) at *T*=0. SCM occurs due to the presence of short range order at finite temperatures in the neighbourhood of this order transition. Slow relaxation in chains of AF coupled spins relies on the relaxation of the staggered magnetization.

In the infinite chain regime (i.e, when the size of magnetic domains separated by two domain walls is smaller than the distance between defects, $2\xi < L$), the relaxation time in the reciprocal space is given by the expression:

$$\tau(q_0) = \frac{\tau_i}{2}\exp\left((2\Delta_\xi + \Delta')/k_B T\right), \qquad [22]$$

with $q_0 = \pi / a$. Here a is the crystallographic distance between magnetic ions, and τ_i describes the intrinsic dynamics of the spin in contact with the thermal bath; $\Delta_\xi = 4\left|J^*\right|S_z^{*2}$ is the energy of a domain wall and Δ' the ion's anisotropy energy. This dynamics can be only determined by NMR or neutron diffraction experiments, sensing the reciprocal space.

Remarkably, the dynamics of finite chain AF coupled spins can be directly observed by ac susceptibility measurements. This is because the reversal of the staggered magnetization of chain segments containing an *odd* number of spins results in a net magnetic moment flip between $+\mu$ and $-\mu$ (the moment of just one ion).

Thus, in the finite size regime (when $2\xi > L$), the relaxation time is expected to follow an Orbach temperature dependence:

$$\tau_{SCM} = \tau_{0,SCM}\,exp\left(E_{SCM} / k_B T\right), \qquad [23]$$

with activation energy:

$$E_{SCM} = \Delta_\xi + \Delta', \qquad [24]$$

where in the non-Kramers case Δ' equals the zero-field splitting (ZFS) gap Δ between the quasi-doublet states. In the particular case of our {Tb(α-fur)$_3$} complex, two different activation energies are expected, since there are two different types of chains, with Tb(III) A and B (Fig. 3) .

Phonon bottleneck effects

The phonon-bottleneck effect (BE) is known to be an important factor affecting the observed relaxation times for spin reversal at very low temperatures. It takes place when the energy of the lattice modes generated by the relaxing spins is not released into the thermal bath sufficiently fast. BE affects differently the various relaxation mechanisms.

Direct processes can be severely affected by BE. Based on thermodynamic arguments it is found that the observed spin bath relaxation time ($\tau_{d,BE}$) depends on the ratio between the magnetic heat capacity at the experimental field *H* (C_H) and the heat capacity contribution of the resonant lattice mode absorbing the phonon emitted by the spin system (C_L)[39]:

$$\tau_{d,BE} = \tau_{sl} + \frac{C_H}{C_L}\tau_{lb}, \qquad [25]$$

where τ_{sl} is the spin lattice relaxation time. Low relaxation rates are specially affected[40].

The Raman process is hardly affected by BE[41], while for Orbach processes, the BE simply renormalizes the prefactor of the relaxation time, but does not modify the activation energy of the exponential dependence[41].

Static magnetic properties

Magnetization

The magnetization of a powdered sample in oil measured at 1.8 K as a function of the applied field, $M(H)$, is shown in Fig. 5. The experimental data could be well fitted using MAGPACK software[42] with g_z*≈18.0(1), in good agreement with the calculated prediction for an angular random distribution of uniaxial grains, with g_z*≈17.8(1), effective spin S*=1/2 and a van Vleck contribution, χ_{VV}=0.022 μ_B/kOe without any Tb-Tb interaction. At this temperature the effect of intrachain and interchain interactions is therefore not perceived.

DC susceptibility

Susceptibility measurements as a function of the temperature in the 300-1.8 K range are shown in Fig. 6. The χT product per mol of Tb atoms at room temperature is 11.68 mol.K/emu, which is close to the expected value of $C = g_J^2 J(J+1)/8$ = 11.8 mol.K/emu for a free Tb(III) ion ($^7F_6$, S=3, L=3, J=6, g_J=3/2). By decreasing the temperature, the χT initially decreases until reaching a step value of 9.6 mol.K/emu ca. 6.4 K, and then rapidly decreases to 8.7 mol.K/emu at 1.8 K. This decrease can be explained as caused by the depopulation of the Tb LF energy levels and the presence of AF intradimer and interdimer exchange interactions.

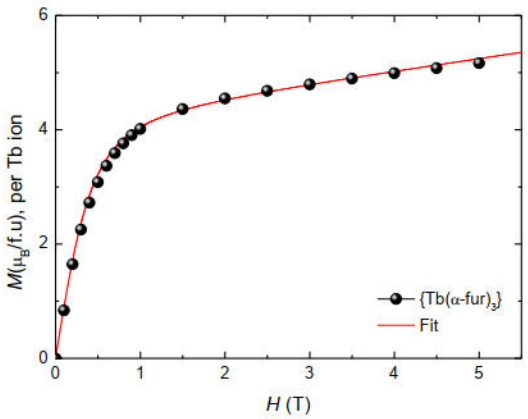

Fig. 5. Dc magnetization as a function of the applied field, $M(H)$, measured at 1.8 K. The data have been fitted using MAGPACK software with an average, dimer Ising model with S*=1/2, g_z*=18.0(1), a van Vleck contribution: $M_{VV}=\chi_{VV}H$, with χ_{VV} =0.022 μ_B/kOe and no interaction.

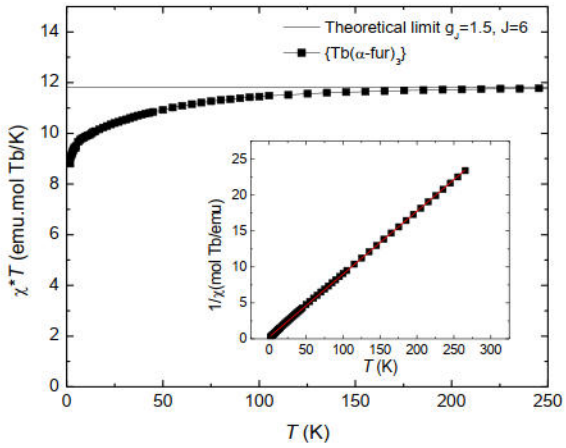

Fig. 6. Dc susceptibility-temperature product (χT) of powdered {Tb(α-fur)$_3$} sample; inset: inverse of the susceptibility *vs.* temperature.

Furthermore, ac susceptibility measurements at very low frequency (f=0.3 Hz) were performed on a powdered sample down to T=15 mK in a dilution refrigerator. The obtained $\chi'(T)$ curve, Fig. 7, can be considered as a good approximation to the static susceptibility and provide further information on intrachain and interchain interactions. The experimental data were scaled to absolute values measured by SQUID in the range 1.8 K to 3 K. They show a rounded susceptibility that can be fitted very well with the prediction (Eq. 10-12) for the powder susceptibility of an AF S*=1/2 linear chain with intrachain exchange interaction between nearest neighbors (z=2) J^*/k_B=-0.135 K (Fig. 7, blue line) and interchain interaction $\left|z_3 J_3^*\right| = 0.127K$. The presence of the single ion ZFS due to the non-Kramers character of Tb(III) does not seem to affect this fitting. This peculiar property was expected for an uniaxial anisotropy in the z direction (parallel to the b-axis)[35] but has not been proven for an anisotropy term such as $\Delta\hat{S}_\perp^*$ in the single ion Hamiltonian.

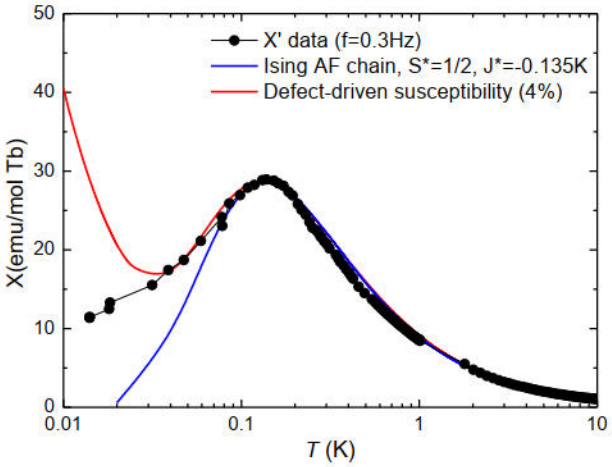

Fig. 7. In-phase ac susceptibility as a function of the temperature at very low frequency (f=0.3 Hz); Blue line: prediction for an Ising S*=1/2 AB chain with J^*/k_B=-0.135 K; Red line: susceptibility driven by a concentration c=4% of defects in the chain[4].

Below T=0.08 K the experimental χ' departs from the equilibrium theoretical prediction. Since $g_x^*=g_y^*=0$, this extra contribution is not caused by a perpendicular contribution to χ', $\chi_\perp$. However, it has been shown that the presence of defects break the chains into finite size lengths which if containing an odd number of spins, may bear an uncompensated moment (see schematics in Fig. 3). They give rise to a non-zero $\chi_\parallel$ proportional to the concentration of defects[4]. From the fitting of the $\chi'(T)$ data to Eq. [23] and the value of χ'_{powder}=10 emu/mol, at T=1.5×10^{-2}K, we estimate c≈0.02-0.04; i.e. the departure from the ideal Ising chain behavior at very low temperature is caused by 2-4% of defects which induce finite size effect in the static susceptibility (Fig. 7, red line).

Heat capacity

The temperature dependence of the heat capacity (HC) was measured between 0.3 K and 45 K under different magnetic fields using a commercial Physical Properties Measurement System (PPMS). The HC in H=0 (Fig. 8a) is practically featureless, though a broad peak at low temperatures is hinted. It is consistent with the model described above for a transverse Ising S*=1/2 AF chain. The HC calculated with Eq. [14], using an intrachain coupling of J^*=-0.135K and the *ab initio* determined ZFS gaps Δ_A and Δ_B gives a rounded peak that falls below the lowest measured temperature (Fig. 8b, dashed lines). However, considering the Δ_A and Δ_B values that have been experimentally deduced from dynamic measurements (*vide infra*), and assuming an equal contribution to the HC of A and B chains, the observed HC is at least qualitatively explained (Fig. 8b).

The magnetic contribution $C_m(T)$ at different applied fields, obtained after subtracting the lattice contribution to the HC data is shown in Fig. 8c. As field increases, a maximum appears at low temperature that shifts to a larger T_{max}. This maximum can be readily explained as the contribution due to the Zeeman splitting of the ground quasi-doublet. At very low temperatures and high field (6 kOe), an upturn in the heat capacity data due to the hyperfine contribution is visible. No sign of long-range ordering is observed down to the lowest temperature measured (0.3 K). The experimental data at 6 kOe could be excellently fitted including a dipolar hyperfine constant of A^*/k_B =0.15 K$^{-\alpha}$ (in S*=1/2), or A/k_B =0.0103K$^{-\alpha}$ (in J=6). This value agrees well with the value reported in Ref.[34].

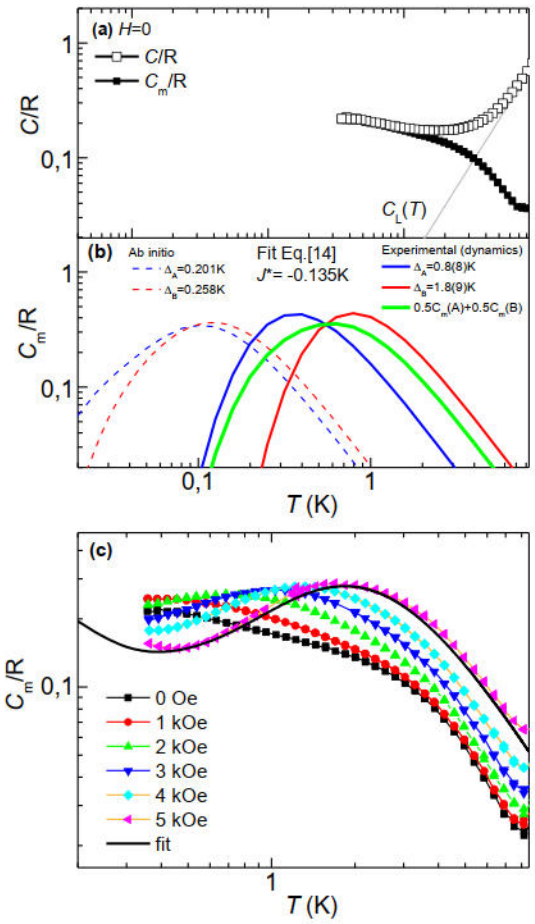

Fig. 8. (a) Heat capacity per mol of Tb atoms as a function of temperature at H=0; the lattice contribution follows the dependence $C_{LT}/R=AT^\alpha$, with A=0.0103K$^{-\alpha}$, α=1.8; b) Theoretical predictions with Eq.[14]; (c) Magnetic contribution to the heat capacity, $C_m(T)$, at different magnetic fields. Fit of the 6 kOe data, considering the electronic and nuclear (hyperfine) contribution.

Dynamic magnetic properties

Zero-field

The in phase $\chi'(T)$ ac susceptibility of {Tb(α-fur)$_3$} measured with the SQUID susceptometer shows no frequency dependence between 1.8 K and 15 K, while the $\chi''(T)$ curves exhibit a small frequency dependence, hinting to slow relaxation at lower temperatures (Fig. S2). For this reason, ac experiments were extended down to lower temperatures (15 mK) with a microSQUID susceptometer installed in a dilution refrigerator[43]. The data are shown in Fig. 9, once they have been scaled to the $\chi'(T)$ SQUID data.

The maximum in $\chi'(T)$ with f=0.33 Hz has been used above to describe the equilibrium (static) susceptibility in terms of an

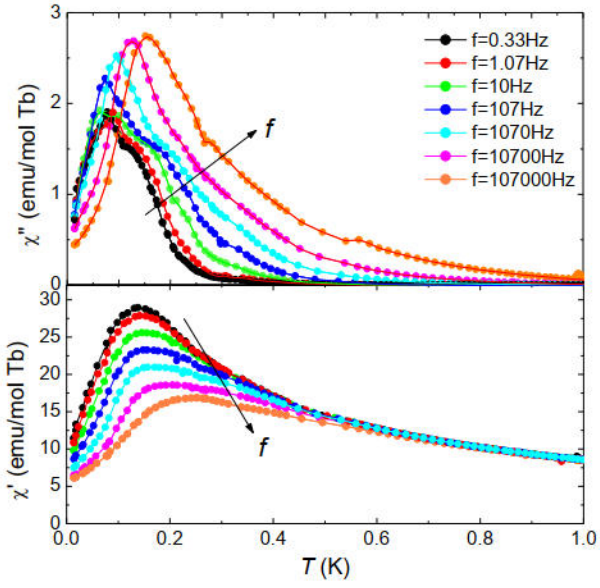

Fig. 9. Out-of-phase $\chi''(T)$ and in-phase $\chi'(T)$ ac susceptibility of {Tb(α-fur)$_3$} measured at zero bias field and varying temperature down to 15 mK.

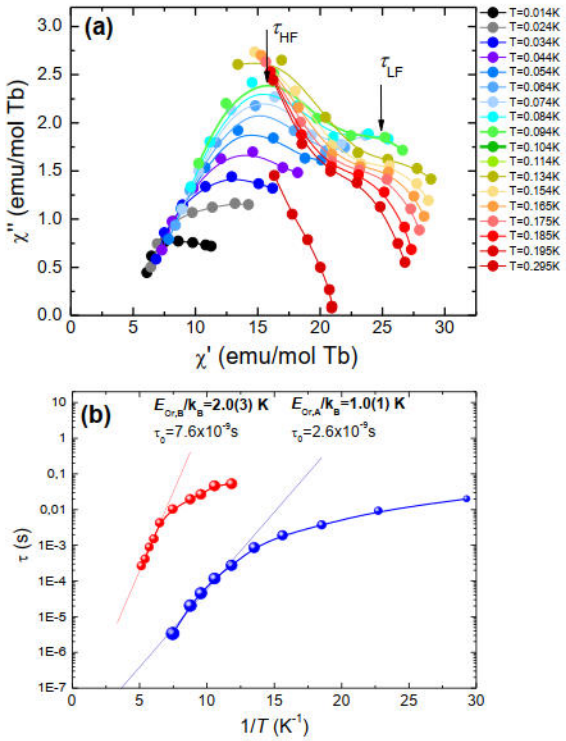

Fig. 10. (a) Cole-Cole plots of some χ', $\chi''(f)$ isotherms measured at very low temperatures (χ',$\chi''(f)$ data in Fig S3); (b) Relaxation times of the two process determined at H=0.

Ising S*=1/2 AF chain (*vide supra*). In Fig. 9 it can be noted that even at this low frequency a non-zero χ''(T), with a rounded maximum appears. Both $\chi'(T)$ and $\chi''(T)$ maxima are shifted to higher temperature for increasing f. At the lower frequencies the presence of a shoulder in $\chi''(T)$ hints towards the presence of two different relaxation processes. This feature becomes more evident in the Cole-Cole plots (Fig. 10a) of some isotherms (Fig. S3).

From the position of the maxima in the Cole-Cole plots, the relaxation times of the two processes have been determined. They are shown in Fig. 10b as a function of the reciprocal temperature. The two relaxation processes follow an Orbach-type temperature dependence, with activation energies $E_{Or,A}/k_B$=1.0(1) K and $E_{Or,B}/k_B$=2.0(3) K. As temperature is lowered, the slope of the lnτ *vs.* 1/T decreases progressively.

The defects in the chain play an essential role on the magnetization dynamics, as they break the spin chains into segments of different lengths. If the average length of these segments is L, slow magnetic relaxation processes can be associated with the motion of the domain walls in the AF Ising chains, while $2\xi<L$ (high-T limit), and with the flipping of chain segments with odd number of Tb ions when $2\xi>L$ (low-T limit). The two different slopes are then associated to the two different types of existing chains, Tb(A) and Tb(B). This picture is schematized in Fig. 3. Indeed, as described earlier, the relaxation time of such a chain is expected to have an Orbach relaxation with an activation energy (Eq. 24), $E_{SCM}=\Delta_\xi+\Delta$, encompassing the activation energy arising from exchange interaction and that arising from the ZFS energy of the non-Kramers quasi-doublet. In this case, taking into account that J^*/k_B=-0.135 K, the exchange contribution is $\Delta_\xi/k_B=4|J^*|S_z^{*2}=0.135K$, thus it is deduced from the dynamic experiments that Δ_A/k_B=0.8(8) K and Δ_B/k_B=1.8(9) K for Tb(A) and Tb(B) sites, respectively. These values are of the order, but larger than those calculated by *ab initio* calculations. The small discrepancy may come from the simple approximation used for the AF SCM Ising model, but also from the low precision of the calculated energy eigenvalues in this case.

As temperature is decreased below 0.14 K (A), 0.08 K (B), the slope of ln$\tau(T)$ *vs.* 1/T reduces towards values of τ_D~0.1 s (A), τ_D~0.02 s (B). Usually, this tendency has been interpreted

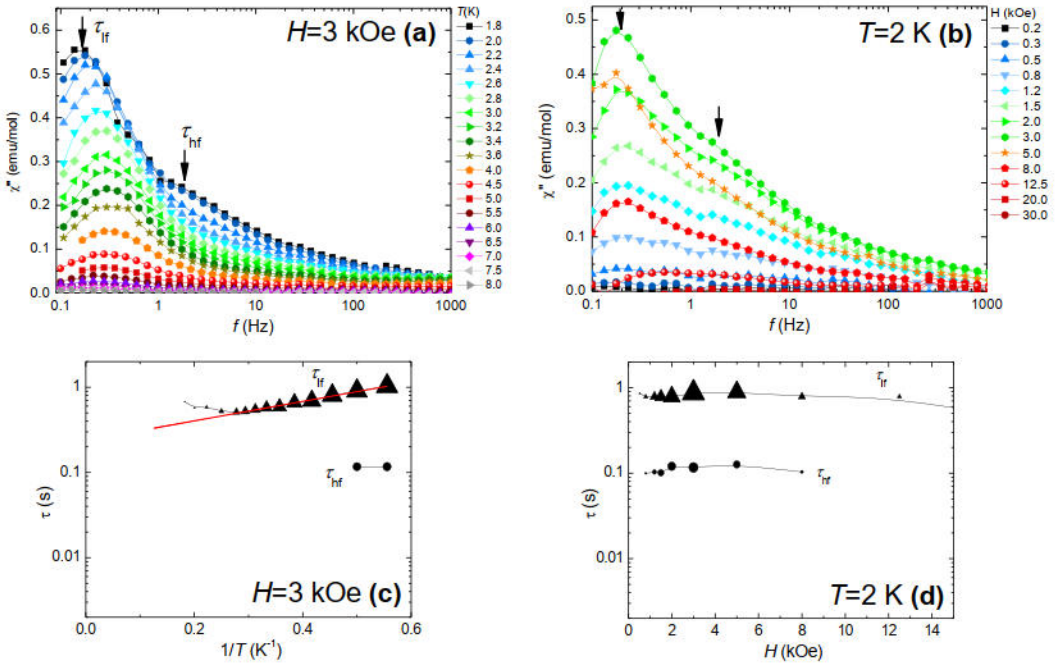

Fig. 11. Ac susceptibility results in H≠0. (a) $\chi''(f)$ at different temperatures, at constant H=3 kOe; (b) $\chi''(f)$ at different applied fields, at T=2K; (c) relaxation time vs. inverse of the temperature, at H=3 kOe; (d) relaxation time as a function of the applied field, at T=2 K.

in lanthanides as an evidence of tunnelling process between the two states of the ground doublet. However, the experimental relaxation times are too large for tunnelling. Instead, since we are dealing with very low temperatures and a split quasi-doublet, it is more likely that such relaxation stems from a direct process between the two states of the quasi-doublet[37]. We do not expect phonon-bottleneck (BE) effects in these measurements, since the sample is in direct contact with the ^{3}He-^{4}He bath. Unluckily, the values of Δ could not be determined in this experiment using Eq. 18.

In summary, {Tb(α-fur)$_3$} linear complex exhibits defect mediated SCM behavior in the two types of existing chains at low temperatures 0.1<T<1 K; 1D long-range ordering that would eventually develop at T=0 due to critical slowing down is precluded by the presence of defects. Instead, below ~0.1K slow relaxation proceeds through SIM direct processes.

Non-zero applied field

We performed χ', $\chi''(f, H)$ measurements as a function of the applied field at 2.0 K; in addition, χ', $\chi''(f, T)$ data were recorded at the optimum field, H=3 kOe, such that the $\chi''(H)$ intensity was maximum (Fig. 11).

Two very slow relaxation processes can be observed, one with high intensity χ'' peak at low frequencies, and another one of lower intensity at higher frequencies. The relaxation times for the two processes, τ_{lf} and τ_{hf}, as a function of the inverse temperature, $\tau(1/T)$, and as a function of the field, $\tau(H)$, have been derived from the position of the χ'' peaks and are shown in Fig. 11c, d.

Notice that the main relaxation process is a very slow process ($\tau \approx 0.8$ s), and its H dependence is very weak. It is quite similar to very slow processes previously found in all Dy polymeric chains we have studied[10,13]. The field induced slow relaxation has no relation with the SCM behavior detected at H=0. In fact, at $H \neq 0$ it is caused by a direct process affected by strong bottleneck (BE) effect since in the SQUID experiment the thermal contact with the bath through He exchange gas is poor compared with the microSQUID case, where the sample is immersed in the cryogenic liquid.

In order to demonstrate the strong influence of the bath, experiments in the SQUID susceptometer under different gas pressures have been done. As clearly shown in Fig. 12, when the chamber is vented, instead of purged, there is an increase in the thermal contact between the sample and the bath, which increases by two orders of magnitude the relaxation rate.

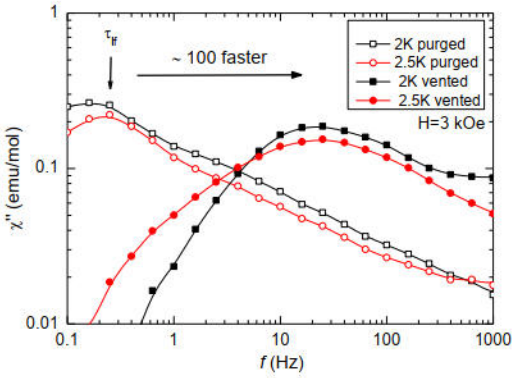

Fig. 12. $\chi''(f)$ at low T=2-3 K, H=3 kOe measured in the SQUID susceptometer under different pressure conditions: experiments were performed with the chamber either purged or vented.

Besides, as explained in the theoretical section, at very low temperature this effect becomes quite relevant at increasing magnetic field since the ratio of magnetic to lattice heat capacity strongly increases (see Fig. 8b). Therefore, no intrinsic magnetic information on the spin relaxation rate can be extracted.

Experimental

General

X-ray diffraction measurements were performed with a Nonius Kappa CCD diffractometer fitted with an Oxford model 700 cryostream cooler.

The magnetization, dc and ac susceptibility of powdered samples were measured, above 1.8 K, using a Quantum Design superconducting quantum interference device (SQUID) magnetometer. Ac measurements were done at an excitation field of 4 Oe, and under dc fields between 0-10 kOe, while sweeping the frequency between 90 and 13330 Hz in the ACMS option of a Quantum Design PPMS. Measurements on powdered samples were performed adding Daphne oil to fix the grains at low temperatures.

Ac susceptibility measurements in the very low temperature range (15 mK - 3.0 K) under zero applied field were performed using a homemade microSQUID[44] housed in the mixing chamber of a ^{3}He-^{4}He dilution refrigerator. The amplitude of the excitation field was h_0=0.25 Oe, and the frequency range 0.33 Hz< f <107 kHz. The output signal in absence of sample is virtually zero[43]. The powdered sample was mixed with a few percent of Apiezon_N grease to enhance the internal thermal contact.

Heat capacity $C(T)$ under different applied fields (0-30 kOe) was measured on a powdered sample embedded in Apiezon grease, using a Quantum Design PPMS.

Fluorescence emission spectra were obtained at 77 K, Liquid Nitrogen Temperature (LNT) by exciting the samples with a 1000 W ORIEL 66187 tungsten halogen lamp and a double 0.22 m SPEX 1680 B monochromator. For the emission spectra, the excitation was carried out at 380 nm ($^5D_3$ level). Fluorescence emission was detected using a 0.5 JARREL-ASH monochromator with a Hamamatsu R928 photomultiplier tube. All optical spectroscopy measurements were corrected from the system response.

Syntheses and analytical data

All chemicals were used as received. Manipulations were performed under aerobic conditions. {Tb(α-fur)$_3$(H_2O)$_3$}$_n$, denoted as {Tb(α-fur)$_3$}$_n$, was prepared using precursors Mg(α-fur)$_2$ (3 mmol) and Tb(ClO_4)$_3$ (3 mmol). An aqueous solution (10 ml) of Mg(α-fur)$_2$ was added to an ethanol solution (10 ml) of Ln(ClO_4)$_3$ with constant stirring for 20 min until the solution becomes transparent. After a week, colorless crystals were collected, washed in ethanol and dried under vacuum. Crystals were obtained in ca. 80% yield. Calc. For ($C_{15}H_{15}O_{12}Tb$)n (1): C, 32.98; H, 2.77;. Found: C,

32.89; H, 2.79; IR (cm^{-1}): 3120b, 1583sh, 1570b, 1471s, 1413s, 1399b, 1230m, 1199s, 1136m, 1074m, 1013m, 932m, 883m, 785b, 755b.

Discussion and Conclusions

The magneto-structural study performed on the new synthesized {Tb(α-fur)$_3$} complex allows to draw the following conclusions:

X ray diffraction evidences that there are two different sites Tb(A) and Tb(B) that can be distinguished by their different coordination caused by the interchange between a water molecule and a dangling ligand. 1D chains of Tb – Tb dimers, connected by carboxylate ligands along the *c*-axis are formed. Chains contain either only Tb(A) or Tb(B) sites. The crystal structure is formed by random stacking along the *a*-axis of 2D supramolecular layers, containing each the same type of chains.

The *ab initio* calculations predict that Tb ion has two different magnetic states for Tb(A) and Tb(B). The ground state is highly anisotropic with the moment oriented approximately perpendicular to the *c*-axis. The gyromagnetic factor for this ion g_z*=18.0(1), determined from magnetization measurements is in excellent agreement with the calculated result g_z*=17.8. The low energy quasi-doublet is actually constituted by two singlets separated by a small energy difference, as expected for a non-Kramers ion such as Tb, with even number of electrons at the 4f orbital. The calculated energy difference from the quasi-doublet to the next excited states is consistent with the experimental LN emission spectrum, 185.9 K and 168.8 K for Tb(A) and Tb(B), respectively.

The static magnetic properties of the {Tb(α-fur)$_3$} compound can be described in terms of the ABC Ising S*=1/2 model. The Ising character is imposed by the strong anisotropy of the ground state. The intradimer and interdimer interactions can be considered to be identical, in view of the very small difference in Tb-Tb distances; thus, the complex behaves magnetically as an AF Ising chain with intrachain coupling J^*/k_B=-0.135 K. Though formally the fictitious S*=1/2 model for the non-Kramers Tb(III) chain is actually the transverse Ising chain (TIC), the ground quasi-doublet ZFS effects could not be detected in the static properties measured in this work. At very low temperatures, the presence of a non-zero susceptibility reveals the presence of defects in the chains, in estimated concentration ~2-4%.

Slow relaxation dynamics observed at very low temperatures, 0.1<*T*<1K, under *H*=0 can be in fact explained by defect-mediated SCM behavior occurring in the two different types of AF chains present in the compound. The mechanism allowing SCM is the segmentation of the chains by defects in pieces containing an odd number of spins. The two SCM processes are Orbach-type with energies, $E_{Or,A}/k_B$=1.0(1) K, $E_{Or,B}/k_B$=2.0(3) K. The activation energy stems from two terms, $E_{SCM} = \Delta_\xi + \Delta$: in the two chains Δ_ξ ≈0.135K is identical, while the Δ values are different, and experimentally determined to be 0.8(8) K (A) and 1.8(9) K (B). These values are compatible with *ab initio* predictions, within the calculation error. By decreasing the temperature, there is a slowing down of the relaxation time due to the increase of the correlation length, but long-range ordering is precluded by the presence of defects. At very low temperatures, *T*<0.1 K, SCM behavior is replaced by SIM slow relaxation via direct processes between the quasi-doublet states. At $H \neq 0$ two slower relaxation processes set on even at higher temperatures, which are assigned to direct processes, affected by severe phonon bottleneck effects.

It is interesting to compare the relaxation behavior of the present complex {Tb(α-fur)$_3$} **(1)** with that of the previously reported, structurally similar complex {Dy(α-fur)$_3$}$_n$ **(2)** based on a Kramers ion. In both cases, the structure is formed by stacking of 2D layers containing either Ln(A) or Ln(B) types of chains. The two different sites A and B in compounds **(1)** and **(2)** play an essential role in the magnetic properties, albeit in a different way. In complex **(1)** spins are perpendicular to the chain and AF coupled, while in complex **(2)** spins were slightly canted with respect to the *c*-chain direction, there was ferromagnetic intrachain coupling and AF interchain coupling. Slow relaxation occurred at *H*=0 via SIM Thermally Activated Quantum Tunnelling (TAQT) in the two different types of Dy sites, mediated by the excited energy level. In contrast, thermally activated SIM processes are not observed in complex **(1)**. Actually, according to our *ab initio* calculations E_2-E_1/k_B ≈ 180 K so, if one assumes a similar $\tau_0 = 10^{-9}$ s, as found in complex **(2)**, such processes fall beyond our detection frequency window; moreover, the occupation probability of the second excited level in the studied temperature region, $p_{occu}(T=3\ K)=10^{-10}$, is too small for the this type of process to occur.

By decreasing the temperature, slow relaxation via TAQT in **(2)** was replaced by quantum tunnelling (TQM), enabled in the Kramers compound by perturbations splitting the ground state doublet. In the present complex **(1)** no tunnelling process is detected; in spite that non-Kramers ions favor tunnelling through the ground level, the ZFS between the two ground levels is too large to allow QTM and, besides, it enhances the rate of direct processes.

By further decreasing temperature, 3D long-range ordering was established in complex **(2)**, enabled by sufficiently large AF dipolar interchain interactions. In contrast, in complex **(1),** short range ordering enables SCM behavior, but as *T* is decreased and the correlation length increases SCM is no longer sustained (it becomes blocked), and slow relaxation proceeds by individual ion relaxation through direct process.

Under $H \neq 0$ very slow relaxation through direct processes affected by BE were measured in **(2)**, like in complex **(1)**, but in that case Orbach processes through excited states were also available. It is clear from the comparison of the two complexes that the nature of the lanthanide (Kramers or not) brings along drastic changes in the overall relaxation behavior.

Finally, we emphasize that unless very low temperature measurements had been done, {Tb(α-fur)$_3$} complex would have been classified as a "field-induced slow relaxation" type. Only at very low temperatures the intrinsic SCM relaxation at *H*=0 was unveiled. This is a call of attention to many wrong results reported in the literature. The present work demonstrates that very weak interactions can play a central role in determining the dynamical behavior of magnetic systems.

Acknowledgements

This work has been financed by MECOM Projects MAT11/27233-C02-02, MAT2012-38318-C03, MAT2014-53921-R, DGA IMANA E34 and MOLCHIP E98 Projects. Consolider Nanoselect (CSD2007-00041) and by a grant of the Ministry of National Education, CNCS – UEFISCDI, project number PN-II-ID-PCE-2012-4-0261. D.P. thanks the Alexander von Humboldt (AvH) Foundation for financial support. J.L. thankfully acknowledges the resources from the supercomputer "Caesaraugusta" (node of the Spanish Supercomputer Network), technical expertise and assistance provided by BIFI – Universidad de Zaragoza.

Notes and references

1 N. Ishikawa, M. Sugita, T. Ishikawa, S. Y. Koshihara and Y. Kaizu, *J. Am. Chem. Soc.*, 2003, **125**, 8694–8695.

2 J. F. Bartolomé, Juan; Luis, Fernando; Fernández, Ed., *Molecular Magnets*, Springer, 2014.

3 W.-X. Zhang, R. Ishikawa, B. Breedlove and M. Yamashita, *RSC Adv.*, 2013, **3**, 3772.

4 C. Coulon, V. Pianet, M. Urdampilleta and R. Clérac, *Struct. Bond.*, 2015, **2**, doi: 10.1007/430_2014_154.

5 S. Dhers, H. L. C. Feltham and S. Brooker, *Coord. Chem. Rev.*, 2015, **296**, 24–44.

6 S. V Eliseeva and J.-C. G. Bünzli, *Chem. Soc. Rev.*, 2010, **39**, 189–227.

7 C. Coulon, R. Clérac, W. Wernsdorfer, T. Colin and H. Miyasaka, *Phys. Rev. Lett.*, 2009, **102**, 2–5.

8 P. Hu, X. Wang, Y. Ma, Q. Wang, L. Li and D. Liao, *Dalton Trans.*, 2013, **43**, 2234–43.

9 X. L. L. Ying Wang, T. W. Wang, Y. Song and X. Z. You, *Inorg. Chem.*, 2010, **49**, 969–976.

10 E. Bartolomé, J. Bartolomé, S. Melnic, D. Prodius, S. Shova, A. Arauzo, J. Luzón, F. Luis and C. Turta, *Dalton Trans.*, 2013, **42**, 10153–71.

11 a Arauzo, a Lazarescu, S. Shova, E. Bartolomé, R. Cases, J. Luzón, J. Bartolomé and C. Turta, *Dalton Trans.*, 2014.

12 C. Turta, S. Melnic, M. Bettinelli, S. Shova, C. Benelli, A. Speghini, A. Caneschi, M. Gdaniec, Y. Simonov, D. Prodius and V. Mereacre, *Inorganica Chim. Acta*, 2007, **360**, 3047–3054.

13 E. Bartolomé, J. Bartolomé, S. Melnic, D. Prodius, S. Shova, a Arauzo, J. Luzón, L. Badía-Romano, F. Luis and C. Turta, *Dalton Trans.*, 2014, **43**, 10999–1013.

14 R. Sessoli and A. K. Powell, *Coord. Chem. Rev.*, 2009, **253**, 2328–2341.

15 P. Robaschik, M. Fronk, M. Toader, S. Klyatskaya, F. Ganss, P. F. Siles, O. G. Schmidt, M. Albrecht, M. Hietschold, M. Ruben, D. R. T. Zahn and G. Salvan, *J. Mater. Chem. C*, 2015, **3**, 8039–8049.

16 M. Urdampilleta, S. Klayatskaya, M. Ruben and W. Wernsdorfer, *ACS Nano*, 2015.

17 D. Aguilà, L. a. Barrios, F. Luis, A. Repollés, O. Roubeau, S. J. Teat and G. Aromí, *Inorg. Chem.*, 2010, **49**, 6784–6786.

18 C. R. Ganivet, B. Ballesteros, G. de la Torre, J. M. Clemente-Juan, E. Coronado and T. Torres, *Chem. - A Eur. J.*, 2013, **19**, 1457–1465.

19 S. Osa, T. Kido, N. Matsumoto, N. Re, A. Pochaba and J. Mrozinski, *J. Am. Chem. Soc.*, 2004, **126**, 420–421.

20 J. D. Rinehart, M. Fang, W. J. Evans and J. R. Long, *J. Am. Chem. Soc.*, 2011, **133**, 14236–14239.

21 K. Bernot, L. Bogani, A. Caneschi, D. Gatteschi and R. Sessoli, *J. Am. Chem. Soc.*, 2006, **128**, 7947–7956.

22 E. Pasca, T. Roscilde, M. Evangelisti, E. Burzurí, F. Luis, L. J. de Jongh and S. Tanase, *Phys. Rev. B*, 2012, **85**, 184434.

23 F. Branzoli, M. Filibian, P. Carretta, S. Klyatskaya and M. Ruben, *Phys. Rev. B - Condens. Matter Mater. Phys.*, 2009, **79**.

24 M. O. Rodrigues, J. D. L. Dutra, L. A. Nunes, G. F. de Sa, W. M. de Azevedo, P. Silva, F. A. A. Paz, R. O. Freire and S. A. Junior, *J. Phys. Chem. C*, 2012, **116**, 19951–19957.

25 M. Zhu, J. Wang, M. Yang, Y. Ma and L. Li, *Dalton Trans.*, 2015, **44**, 9815–22.

26 R. Liu, C. Zhang, X. Mei, P. Hu, H. Tian, L. Li, D. Liao and J.-P. Sutter, *New J. Chem.*, 2012, **36**, 2088.

27 X. Wang, M. Zhu, J. Wang and L. Li, *Dalton Trans.*, 2015, **44**, 13890–6.

28 2003. CrysAlis RED, Oxford Diffraction Ltd., Version 1.171.36.32, *Dalt. Trans.*, 2014, **43**, 13349–13357.

29 O. V. Dolomanov, L. J. Bourhis, R. J. Gildea, J. a K. Howard and H. Puschmann, *J. Appl. Crystallogr.*, 2009, **42**, 339–341.

30 G. M. Sheldrick, *Acta Cryst.*, 2008, **A64**, 112–122.

31 B. O. Roos and P.-Åke Malmqvist, *Phys. Chem. Chem. Phys.*, 2004, **6**, 2919.

32 F. AQUILANTE, L. DE VICO, N. FERRÉ, G. GHIGO, P.-Å. MALMQVIST, P. NEOGRÁDY, T. B. PEDERSEN, M. PITONÁK, M. REIHER, B. O. ROOS, L. SERRANO-ANDRÉS, M. URBAN, V. VERYAZOV and R. LINDH, *J. Comput. Chem.*, 2010, **31**, 224–247.

33 J. S. Griffith, *Phys. Rev.*, 1963, **132**, 316–319.

34 N. Ishikawa, M. Sugita and W. Wernsdorfer, *Angew. Chemie - Int. Ed.*, 2005, **44**, 2931–2935.

35 I. Chatterjee, *Phys. Rev. B*, 1985, **31**, 3158–3160.

36 S. Katsura, *Phys. Rev.*, 1962, **127**, 1508–1518.

37 R. Orbach, *Proc. R. Soc. A Math. Phys. Eng. Sci.*, 1961, **264**, 485–495.

38 R. J. Glauber, *J. Math. Phys.*, 1963, **4**, 294–307.

39 A. Abragam and B. Bleaney, in *Electron Paramagnetic Resonance of Transition Ions*, 1970, pp. 4, 42, 133–163, 398–406, 417–430,541– 547, 583–599.

40 G. J. Gerritsma, J. Flokstra, G. A. Hartemink, J. J. M. Scholten, A. J. W. A. Vermeulen and L. C. van der Marel, *Phys. B+C*, 1978, **95**, 173–182.

41 P. L. Scott and C. D. Jeffries, *Phys. Rev.*, 1962, **127**, 32.

42 B. M. Properties and I. Neutron, 2000, **3**.

43 E. Bellido, P. González-Monje, A. Repollés, M. Jenkins, J. Sesé, D. Drung, T. Schurig, K. Awaga, F. Luis and D. Ruiz-Molina, *Nanoscale*, 2013, **5**, 12565–73.

44 D. Drung, J.-H. Storm and F. Ruede, *IEEE Trans. Appl. Supercond.*, 2014, **24**, 1600206.